Computational methods in welding and additive manufacturing/Simulation numérique des procédés de soudage et de fabrication additive

Computational modeling of heat transfer and sintering behavior during direct metal laser sintering of AlSi10Mg alloy powder

Mihir Samantaray, Seshadev Sahoo *, Direndranath Thatoi

Department of Mechanical Engineering, Institute of Technical Education and Research, Siksha 'O' Anusandhan (Deemed to be University), Odisha, Bhubaneswar-751030, India

A R T I C L E   I N F O

A B S T R A C T

Direct Metal Laser Sintering (DMLS) is one of the leading additive manufacturing processes, which produces complex metallic parts directly from the powder. One of the major problems of this rapid manufacturing process is an inhomogeneous temperature distribution, which leads to residual stress in the build part. Thus, temperature analyses must be performed, to better understand the temperature distribution and sintering behavior of the powder bed with a different laser recipe. In this study, a comprehensive three-dimensional numerical model was developed to understand the temperature distribution during direct metal laser sintering of AlSi10Mg alloy powder. The computer simulation was carried out in ANSYS 17.0 platform. Further, the effect of process parameters such as laser power and scan speed on the temperature distribution and sintering behavior were studied. From the simulation results, it was found that, when the laser power increased from 70 W to 190 W, the maximum temperature of the molten pool increased from 731 °C to 2672 °C, and the molten pool length changed from 0.286 mm to 2.167 mm. A reverse phenomenon was observed with an increase in scan speed. The sintering depth of the powder layer increases significantly from 0.061 mm to 0.872 mm with increasing the applied laser power, but decreased from 0.973 mm to 0.209 mm as a higher scan speed was applied. The developed model helps to optimize the powder layer thickness and minimize the wastage of excess powders during the sintering process.

1. Introduction

Nowadays, additive manufacturing grabs the attention of academic and industrial communities to produce complex shapes directly from the metallic or alloy powders in a layer by layer fashion. This technology is one of the emerging technologies to build objects with the use of 3-dimensional CAD models [1,2]. Among different types of additive manufacturing processes, Direct Metal Laser Sintering (DMLS) is one of the leading commercial processes for rapid manufacturing of functional prototypes and tools. The process creates solid three-dimensional objects by bonding powdered materials using a high-energy laser beam heat source. The key advantages of this process are its flexibility in materials and shapes, enormous

---

* Corresponding author.
  E-mail address: seshadevsahoo@soa.ac.in (S. Sahoo).

potential for creating complex 3D parts, minimization of wastage of powder materials, and less expense is involved due to the absence of support structures [3,4]. In the DMLS process, a high-energy laser beam interacts with a powder bed and simultaneously melts and consolidates the powders layer by layer. The transient temperature field and the rapid cooling rate are achieved during the interaction between the laser beam and the powder bed, which has a substantial effect on the microstructures and the resultant mechanical properties of the final component. The interaction of the laser beam with the powder bed is accompanied by multiple modes of heat, mass, and momentum transfer that make the process very complex [5]. Even though this process is applied to an extensive range of powder materials and involves rapid melting and sintering phenomena, its scientific and technical aspects are still not well understood.

Recently, many investigations have been carried out to study the temperature phenomena during laser sintering process. Tang et al. [6] have studied the thermal behavior and effects of different process parameters on the quality and accuracy of a three-dimensional solid structure, which was made up of a special copper-based alloy. Simchi [7] had analyzed the effect of processing parameters on the densification of metal powders in the direct metal laser sintering process. He established a relationship between the densification of metal powders and laser energy during direct metal laser sintering, which was found to be very useful for metals or alloys. A transient three-dimensional finite element model has been proposed by Dong et al. [8] to simulate the phase transformation during the laser sintering process by considering thermal and sintering phenomena. Zeng et al. [9] developed a comprehensive thermal model for the selective laser sintering process by using Fourier's heat conduction equation to investigate the temperature distribution on the powder layer. Jian et al. [10] had presented a 3D transient model for simulating the temperature in selective laser sintering process for Al_2O_3 coated with ceramic powder by using a moving CO_2 laser beam. Li and Gu [11] developed a finite element model to predict the relationship between processing parameters and thermal behavior during selective laser melting of AlSi10Mg powder, using the ANSYS 12.0 software. The effects of laser power and laser scan speed on the thermal behavior and the configurations of molten pool were preliminary analyzed, and the corresponding experiments were also conducted to study the microstructure of the build part under different laser processing conditions to verify the reliability of the physical model. Yuan and Gu [12] developed a numerical model for the selective laser melting of TiC/AlSi10Mg nano-composites by using a finite volume method and investigated the effect of process parameters on temperature distribution. A three-dimensional finite element model was proposed by Shi et al. [13] to study the effects of laser power and scan speed on the thermal behavior and melting/solidification mechanism during selective laser melting of the TiC/Inconel 718 powder system. In their study, the authors discussed the formation mechanisms of processing defects like balling effect, pores, microcracks, delamination, etc., in order to optimize the processing parameters. Also, experiments were conducted to validate the model. Hu et al. [14] developed a finite-element model for multi-layer selective laser melting of AlSi10Mg powder. Parametric analysis was carried out under different laser energy inputs. The effect of the laser energy input on the temperature field, the molten pool depth, the cooling rate, and the solidification morphology parameter were also investigated. The simulated results provide valuable theoretical guidance for selective laser melting of AlSi10Mg components. Kundakcioglu et al. [15] investigated the transient thermal analysis for additive manufacturing of 3D complex freeform structures in powder bed systems and laser heat source. The model was able to simulate 3D transient temperature fields in complex structures with changing time and laser path instantaneously, which allow further process enhancements and optimizations for the process in the near future. A novel particle-based discrete element model was developed by Lee et al. [16] to investigate the effects of laser power, laser scan speed, and hatch spacing on the temperature distributions in the powder bed in DMLS process. From their investigation the authors found that, with increasing laser power, the temperature of the powder bed increases, whereas increasing laser scan speed and laser hatch spacing will not affect the average temperature increase in the powder bed. Zhao et al. [17] numerically studied the heat transfer and residual stress evolution in the direct metal laser sintering of Ti alloy by using COMSOL multi-physics environment. Their simulation results reveal the behavior of the melt pool size, temperature history, and change of the residual stresses of the powder layer with variation of the process parameters. The results of the simulation provide a better understanding of the complex thermomechanical mechanisms of laser sintering processes. A finite element model was developed by Dong et al. [18] to simulate the laser sintering of Ti powder bed fusion using the software package ABAQUS. Based on their simulation results, the process parameters can be accurately chosen to avoid the weaknesses of this additive manufacturing technology, such as excessive or insufficient heating. Ojha et al. [19] developed a mathematical model for direct metal laser sintering of AlSi10Mg alloy by considering fluid flow, heat transfer, and solidification characteristics in the liquid pool. Their simulation results give a fundamental understanding of the densification of powder particles in DMLS process.

Despite several advantages of the DMLS process over conventional processes, it still exhibits a few drawbacks due to complex metallurgical phenomena that involve multiple modes of heat transfer. Hence, significant research efforts are required to develop a comprehensive thermal model and to study the relationship between the processing parameters and the thermal behavior. In the present study, a comprehensive thermodynamic model for sintering of AlSi10Mg during a direct metal laser sintering process has been developed on an ANSYS 17.0 platform. Through computer simulation, the thermal behavior of the AlSi10Mg powder layer has been investigated and attention has been given to evaluating the influence of scanning speed and laser power on the molten pool profile, the temperature distribution, and the sintering depth. The simulated results help to optimize the thickness of the powder layer and thereby to reduce the wastage of powder material.
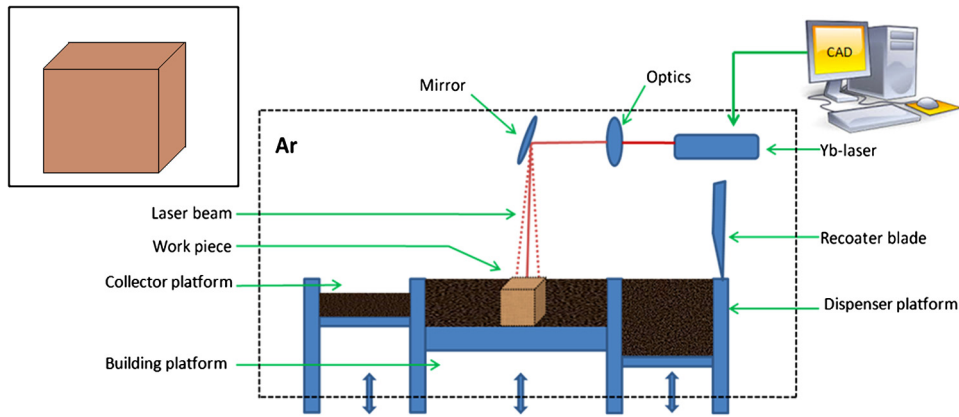
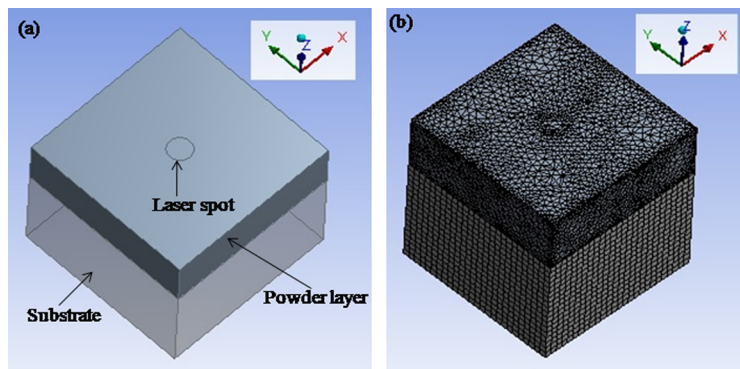**Fig. 1.** Schematic diagram of the DMLS process.

Fig. 2. (a) Computational domain. (b) Finite element model with meshing used for simulation.

2. Computational model for the DMLS process

The current study develops a mathematical model for investigating the thermal behavior during sintering of AlSi10Mg alloy powder in a direct metal laser sintering process. For the development of the model, the following physical assumptions were considered:

 (i) the powder particles are assumed spherical in shape;
 (ii) the powder bed is considered as a continuum;
(iii) the fluid flow is ignored when metal is found in the liquid state;
(iv) the laser beam is assumed to have the Gaussian distribution of the heat source;
 (v) the direction of the laser striking the powder bed surface is always perpendicular to it;
(vi) the powder particles have always homogeneous physical properties in all directions;
(vii) a constant absorption rate is assumed in the modeling scheme;
(viii) perfect thermal contact is assumed between powder bed and substrate;
(ix) temperature-dependent thermo-physical properties of the powders are considered;
 (x) the heat transfer phenomena are dominated by conduction, convection, and radiation;
(xi) the average heat transfer coefficient between the powder bed and the surrounding environment is taken as a constant.

2.1. Physical description of the model

Fig. 1 shows the schematic diagram of the DMLS process and Fig. 2 shows the computational domain considered for the model. The simulation domain consists of the substrate, with dimension 3 mm $\times$ 3 mm $\times$ 2 mm, and a powder layer with dimension 3 mm $\times$ 3 mm $\times$ 1 mm. The laser beam focuses on the top surface of the powder bed with a diameter of 0.2 mm. When the laser beam interacts with the powder layer, heat transfer takes place. It occurs from all surfaces of the powder bed to the surrounding in terms of convection and radiation mode and within the powder bed as well as from the powder bed to the substrate in conduction mode. In this model, the powder bed consists of AlSi10Mg and the substrate is taken as steel.

2.2. Governing equation

Finite element simulations of heat transfer in DMLS processes is carried out by solving a three-dimensional Fourier heat conduction equation, which describes temperature (T) as a function of x, y, z, and time (t). The temperature distribution in the powder bed satisfies the heat conduction equation, which can be expressed as

$$\frac{\partial}{\partial x}\left(k\frac{\partial T}{\partial x}\right) + \frac{\partial}{\partial y}\left(k\frac{\partial T}{\partial y}\right) + \frac{\partial}{\partial z}\left(k\frac{\partial T}{\partial z}\right) + \dot{Q}\,(x,y,z,t) = \rho c_p \frac{\partial T}{\partial t} \tag{1}$$

where k is the effective thermal conductivity of the powder bed, T is the temperature of the powder system, $\dot{Q}\,(x,y,z,t)$ is the rate of the internal heat generation per unit volume within the component, ρ is the material density, C_p is the specific heat capacity, and t is the interaction time between the laser beam and the powder material.

As the laser beam impacts on the top surface of the powder bed, heat generation takes place and it can be modeled in form of heat flux. In this model, the input heat source follows a Gaussian distribution [20]. The mathematical expression of the input heat flux q can be defined by

$$q(r) = \frac{2AP}{\pi r_0^2} e^{-2r^2/r_0^2} \tag{2}$$

where A is the laser absorptance of the powder system, P is the laser power, r_0 is the radius of the laser beam, and r is the radial distance between the laser beam and the center of the spot generated on the top surface of the powder bed.

2.3. Initial and boundary conditions

The initial condition for the temperature distribution throughout the powder bed and substrate at time $t = 0$ is assumed as:

$$T(x,y,z,t)|_{t=0} = T_a = 300 \text{ K} \tag{3}$$

The net amount of heat transfer from each surface except the bottom surface is expressed as:

$$-k\left(\frac{\partial T}{\partial Z}\right) = \varepsilon\sigma\left(T^4 - T_0^4\right) + h(T - T_a) \tag{4}$$

The amount of energy lost to the surrounding from the side surface of the powder bed and the substrate by convection mode is described by

$$q_{\text{con}} = h(T - T_a) \tag{5}$$

where h is the convective heat transfer coefficient, T is the temperature of the top surface of the powder bed, and T_a is the ambient temperature.

The heat loss due to radiation from the powder layer is

$$q_{\text{rad}} = \varepsilon\sigma\left(T^4 - T_0^4\right) \tag{6}$$

where ε is the emissivity of the powder bed, and σ is the Stefan–Boltzmann constant for radiation.

At the bottom surface of the substrate, no heat loss is considered, which is expressed as:

$$\left[k\left(\frac{\partial T}{\partial Z}\right)\right]_{z=0} = 0 \tag{7}$$

3. Results and discussion

3.1. FE simulation of heat transfer in the DMLS process

In the present study, a computational model is developed to investigate the thermal behavior and sintering mechanism of AlSi10Mg alloy in direct metal laser sintering. ANSYS 17.0 is used to solve the above-described heat transfer equation to obtain a thorough understanding of the thermal behavior during the DMLS process. The model takes into account the concurrent heat transfer phenomena, i.e. conduction, convection, and radiation in the powder bed as well as in the substrate. Simulations are carried out for sintering of AlSi10Mg in a powder bed as well as in the substrate. The grid for the computational domain is finalized after a grid independent test. Considering the computational precision and simulation efficiency, a tetrahedral mesh structure was obtained for the powder bed with fine meshing, and a hexahedral mesh for the substrate was obtained with medium meshing. The mesh contains both structured and unstructured mesh. The three-dimensional simulation model has meshed into 23,149 nodes and 76,121 elements in all. The temperature-dependent thermo-physical

Table 1
Thermo-physical properties of AlSi10Mg alloy [21].

Temperature	20 °C	100 °C	200 °C	300 °C	400 °C
Thermal conductivity (k), W/m K	147	155	159	159	155
Specific heat capacity (c_p), J/kg K	739	755	797	838	922
Heat transfer coefficient (h), W/m² K	80				
Density (ρ), g/m³	2.67				
Emissivity (ε)	0.3				

Table 2
Process parameters of the DMLS process.

Parameters	Values
Laser power (W)	70, 100, 130, 160, 190
Scanning speed (mm/s)	100, 200, 300, 400, 500
Laser spot size (mm)	0.2
Thickness of layer (mm)	1
Laser absorptivity	0.95

Table 3
Thermo-physical properties of structural steel [22].

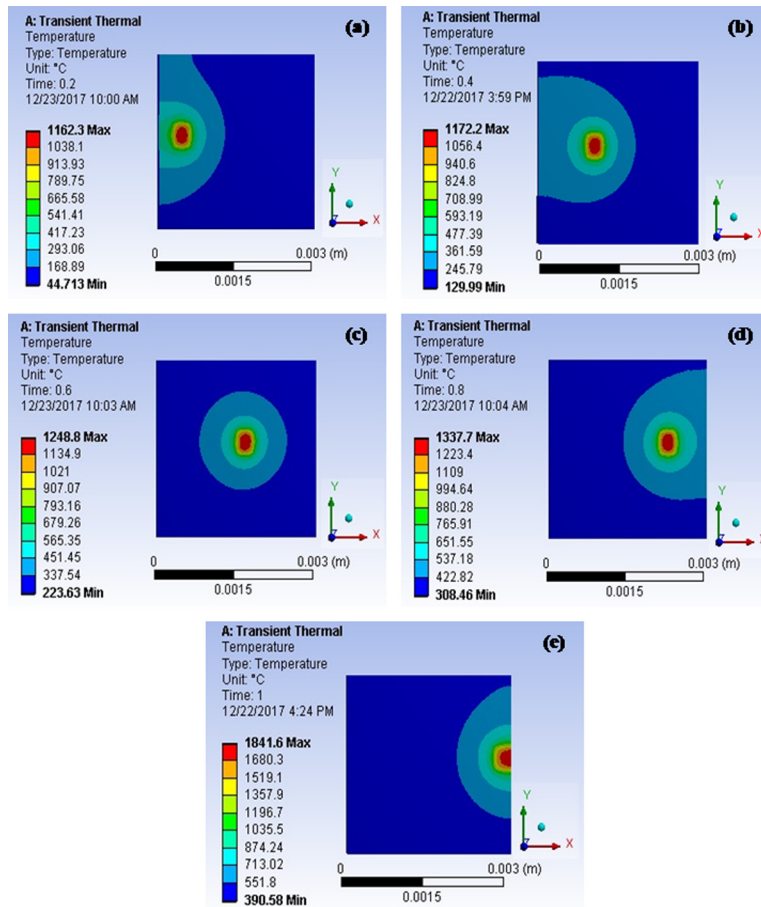| Properties of steel	Values
Thermal conductivity (k), W/m K	60.5
Density (ρ), kg/m³	7850
Specific heat, (c_p), J/kg K	434

Fig. 3. Top view of the thermal profile of AlSi10Mg powder bed at different time steps in the DMLS process.

properties of AlSi10Mg, the thermo-physical properties of the steel, and the processing parameters used for the simulations are given in Tables 1–3.

Fig. 3 shows the top view of the transient temperature profile of the powder bed at different locations on the top surface when the scan speed is 100 mm/s and the laser power is 100 W; Fig. 4 represents the cross-sectional view of the
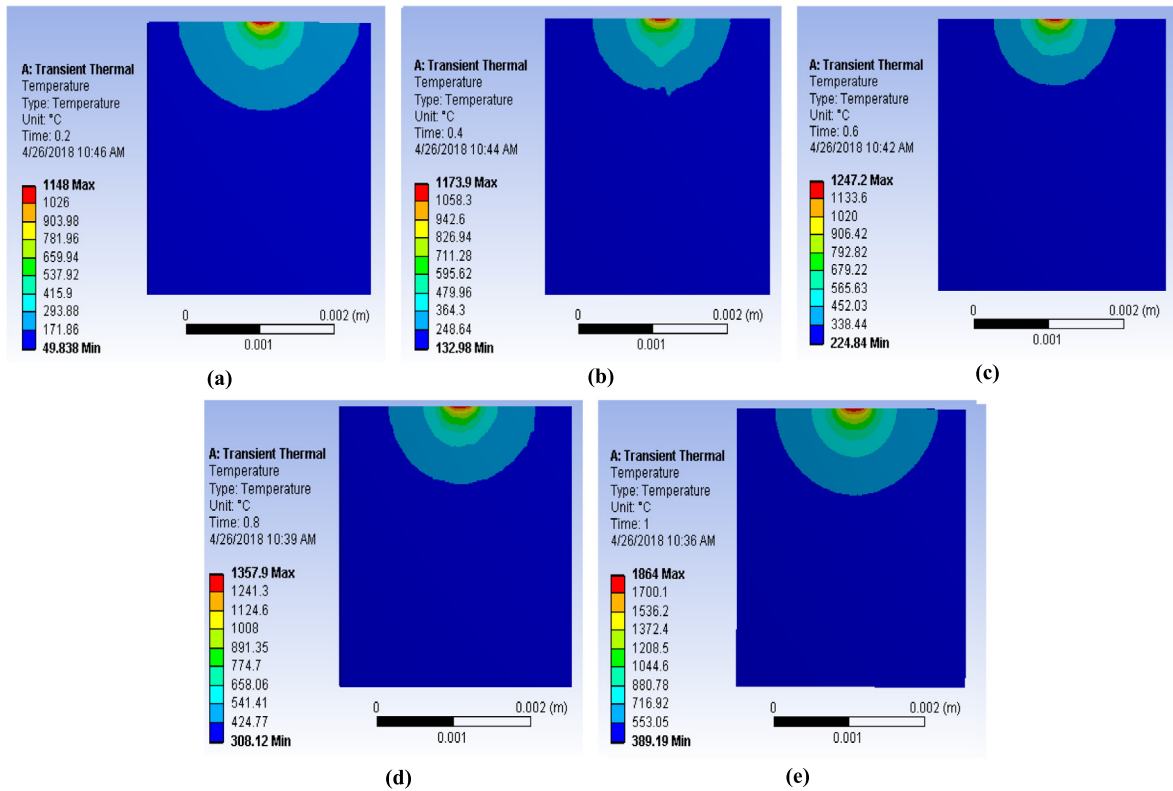
Fig. 4. Vertical cross-sectional view of the thermal profile of AlSi10Mg powder bed at different time steps in the DMLS process.

temperature profile. The temperature distribution in the melt pool region is shown by different colors. The temperature is higher in the center of the melt pool region than in the other regions. The temperature contours on the top surface of the molten pool look like a series of ellipses, and the ellipses are more intensive in the laser scan direction. At the center of the molten pool, the AlSi10Mg alloy powder is in completely liquid form. The maximum temperature of the molten pool at the 2nd, 4th, 6th, and 8th locations is 1162 °C, 1172 °C, 1248 °C, 1337 °C, and 1841 °C, respectively; subsequently, the length and width of molten pool are increased from 0.461 mm to 1.62 mm and from 0.515 mm to 1.683 mm. The temperature in precise locations increases rapidly as the laser beam approaches and decreases sharply as the laser beam moves away from that location. This happened due to a change in thermal conductivity from the powder to the solid layer, which transfers heat quickly to the other regions of the powder bed. Also, the substrate plays a significant role in heat dissipation.

The maximum temperature at the first location is relatively low as compared to the other locations. In DMLS process, when the laser beam moves from one location to nearby one, the maximum temperature and the size of the molten pool increase gradually. This is mainly attributed to the fact that heat stored in the previous location has an influence on the next processing location and, accordingly, this leads to heat accumulation. The repetitive scan of the powder layers results in rapid melting and solidification, which accomplishes a sound metallurgical bonding between the powder particles as well as the adjacent powder layers. So, the liquid-state sintering of the AlSi10Mg powder particles will take place and, as a result, a completely dense build part is produced in the DMLS process.

3.2. Effect of laser power on thermal behavior

The temperature profile of the powder bed during the sintering process can provide useful input for determining the distribution of the thermal stresses and predicting the residual stresses in the build part. Figs. 5 and 6 illustrate the top view of the thermal profile and the cross-sectional view of the heat-penetrated region of the powder bed along the XY plane with varying laser power at 70 W, 100 W, 130 W, 160 W, and 190 W, while keeping the laser scan speed constant at 100 mm/s in all cases.

From the thermal profile, it is observed that there is an enhancement of temperature with increasing the laser power. At a laser power of 70 W, the average maximum temperature in the powder bed is approximately 731 °C, which is above the
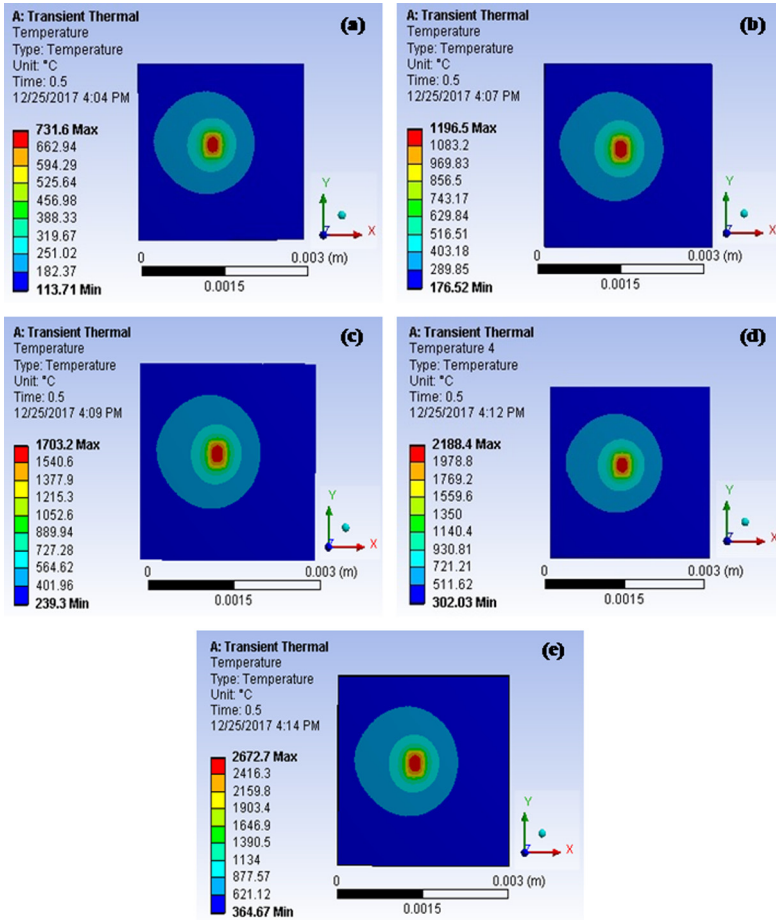
Fig. 5. Top view of the temperature contour of the powder bed for different laser powers: (a) 70 W, (b) 100 W, (c) 130 W, (d) 160 W, and (e) 190 W.

melting point of AlSi10Mg. When the laser power is increased from 70 W to 190 W, the average temperature in the powder bed is changed from 731 °C to 2672 °C, and the temperature gradient is significantly increased along the scan path, which is clearly observed in the thermal profile. As the laser power increases, the beam intensity increases, which increases the heat flux as per Eq. (2). The heat flux is directly proportional to the laser power. So, a high rate of heat transfer will occur from the laser beam to the powder surface, which increases the temperature of the powder layer. The bottom surface of the powder bed is in adiabatic condition, there will be no loss of heat from the bottom surface to the outside, as the thermal gradient vanishes gradually. Hence, no temperature rise can be seen at the bottom wall. A high temperature is obtained in the molten pool region as the laser directly touches the powder bed at that point. The higher value of heat is gradually being transferred to other surfaces of the powder bed as the laser penetrates deeper into it. This is clearly evident from the simulation results.

Fig. 7 shows the dimensions of the molten pool at different laser powers during the DMLS processing of AlSi10Mg alloy. From the figure, it is observed that the length and width of the molten pool are approximately in positive linear relationship with the applied laser power. As the utilized laser power is increased from 70 W to 190 W, noticeable enhancements of the dimensions of the molten pool, i.e. its length (from 0.286 mm to 2.167 mm) and its width (from 0.327 mm to 1.962 mm) are recorded.

Fig. 8 shows the plot of the sintering depth in the powder bed as a function of laser power. From the graph, it is observed that with the increase in laser power, the laser beam intensity increases and thus the sintering depth increases. The sintering depth is measured by using ImageJ software. When the laser power is 70 W, the maximum temperature obtained is 731 °C, and the depth is 0.061 mm; when the laser power is 190 W, the temperature is 2672 °C, and the depth is 0.872 mm. So, it is found that the laser power strongly affects the temperature and sintering depth values in a positive way. Based on the sintering depth, the thickness of the powder layer is optimized as per the requirement for a particular processing condition. So, the wastage of the powders in the DMLS process can be minimized.
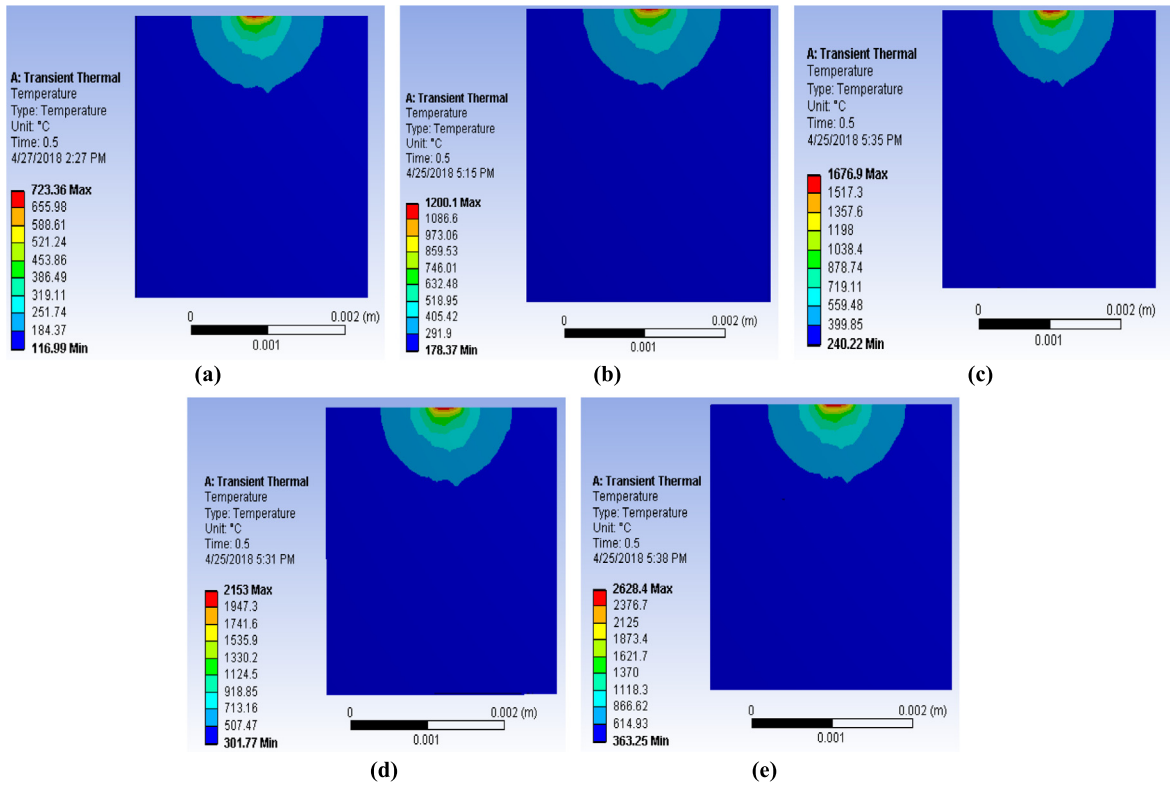
Fig. 6. Cross-sectional view of the heat penetration profile of the powder bed at different laser powers: (a) 70 W, (b) 100 W, (c) 130 W, (d) 160 W, and (e) 190 W.
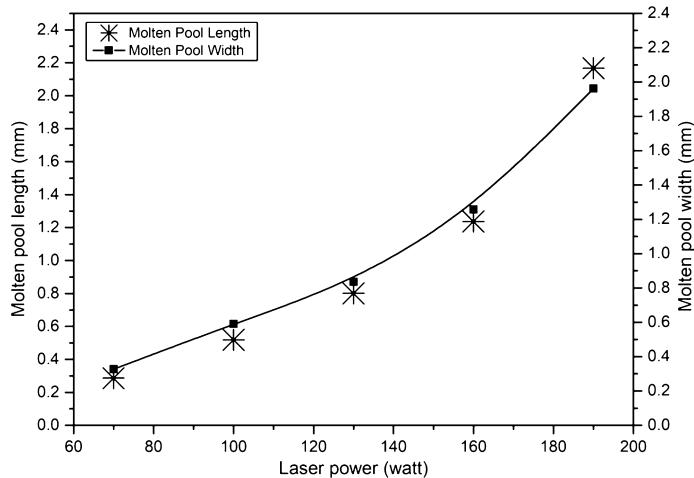

Fig. 7. Variation of the molten pool dimensions with the laser power.

3.3. Effect of scan speed

Fig. 9 shows the top view of the temperature distribution of the powder layer in the DMLS process, when the scan speed varies from 100 mm/s to 500 mm/s, keeping the laser power constant, i.e. 100 W. From the simulation profile, it is observed that with increasing the scan speed, the laser energy density is gradually decreasing, which results in a decrease in temperature. When the scan speed is 100 mm/s, the maximum temperature is 1721 °C and the depth is 3 mm. When the speed is 200 mm/s, the maximum temperature is 1483 °C and the depth is about 0.689 mm. When the laser power and the spot diameter are constant, the interaction time of the laser energy on the powder particles is longer with a lower scanning speed and the sintering temperature is relatively higher for the effects of heat accumulation and heat conduction. On the
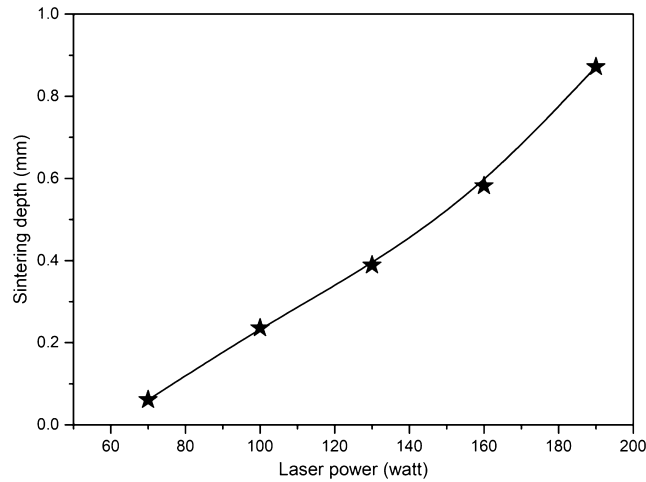
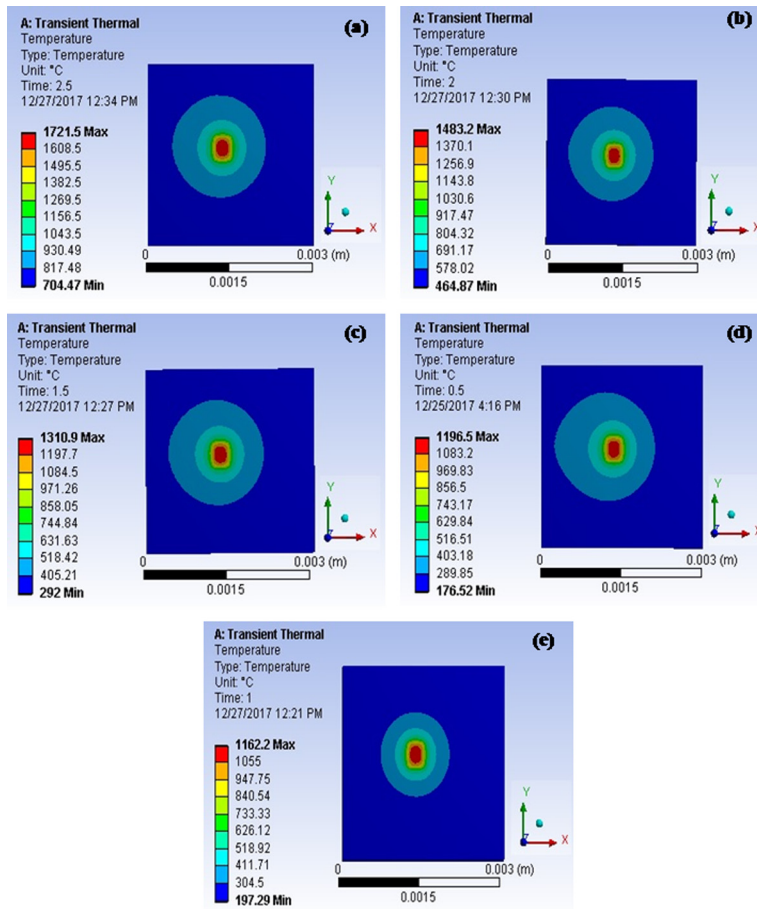**Fig. 8.** Variation of the sintering depth with the laser power.

Fig. 9. Thermal profile of the powder bed at different scan speeds: (a) 100 mm/s, (b) 200 mm/s, (c) 300 mm/s, (d) 400 mm/s, and (e) 500 mm/s.

contrary, the interaction time of the laser energy on the powder particles is shorter with a higher scanning speed and the sintering temperature is relatively lower for the heat transfer around the powder particles with enough time.

Fig. 10 shows The cross-sectional view of the heat penetration profile of the powder bed at different scan speeds. The heat penetration profile gives a clear picture of the temperature variation along the thickness side of the powder bed.

The molten pool's dimension as a function of scan speed is shown in Fig. 11. From the graph, it is observed that the dimensions of the molten pool decrease with the increment of scan speed. When increasing the scan speed from 100 to
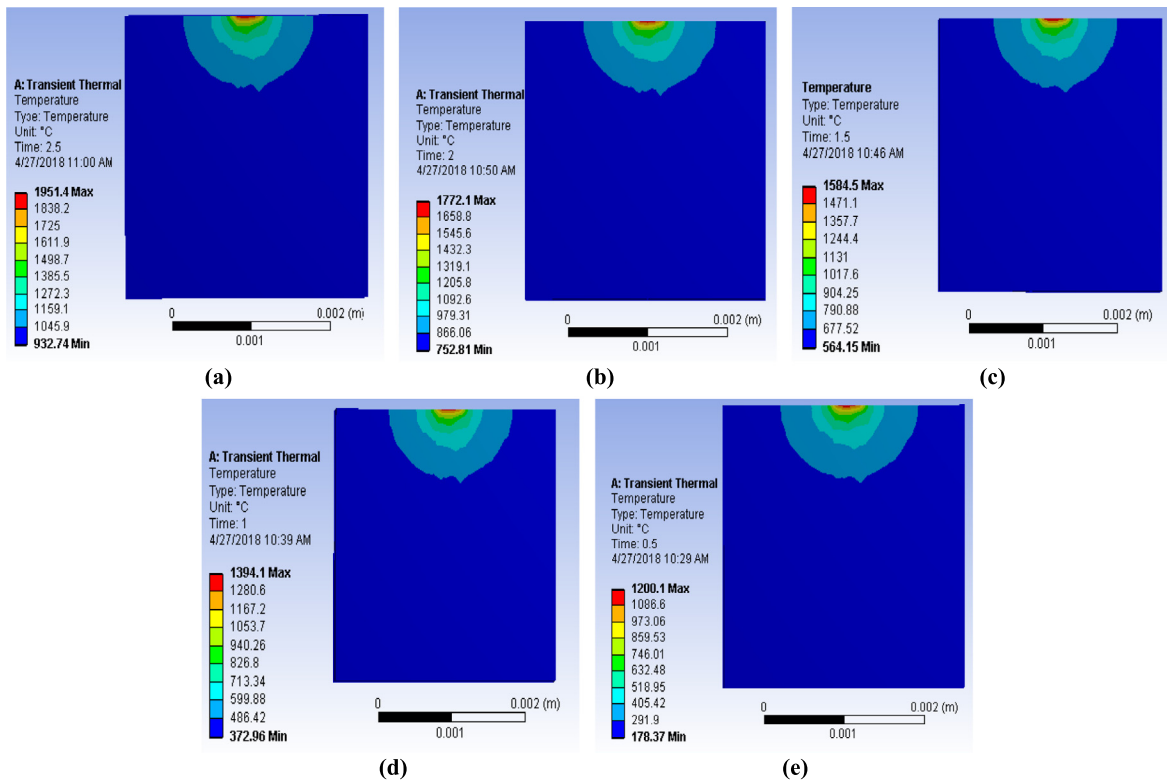
Fig. 10. Cross-sectional view of the heat penetration profile of the powder bed at different scan speeds: (a) 100 mm/s, (b) 200 mm/s, (c) 300 mm/s, (d) 400 mm/s, and (e) 500 mm/s.
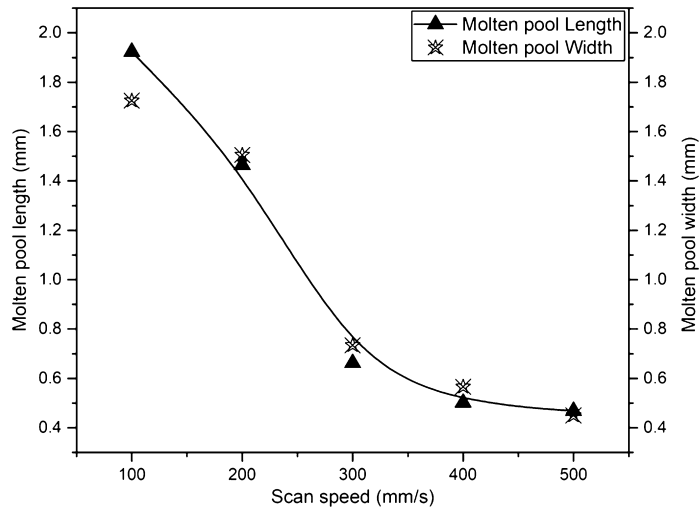

Fig. 11. Variation of the molten pool's dimension with the scan speed.

500 mm/s, the length of the molten pool decreases evidently from 1.923 mm to 0.468 mm. Meanwhile, the width of the molten pool reduces from 1.897 mm to 0.450 mm.

Further, the calculation results manifest that the decreasing tendency becomes less pronounced as the utilized scan speed is increased above 100 mm/s. As scan speed depends on laser energy density, with increasing the former, the density of the latter decreases, and hence the sintering depth is also decreased. This can be clearly seen in Fig. 12.

So, from the simulation results, it is found that sintering depth decreases from 0.973 mm to 0.209 mm with a decrease in the value of the temperature; that is, depth and temperature are directly proportional to each other at different scanning speeds.
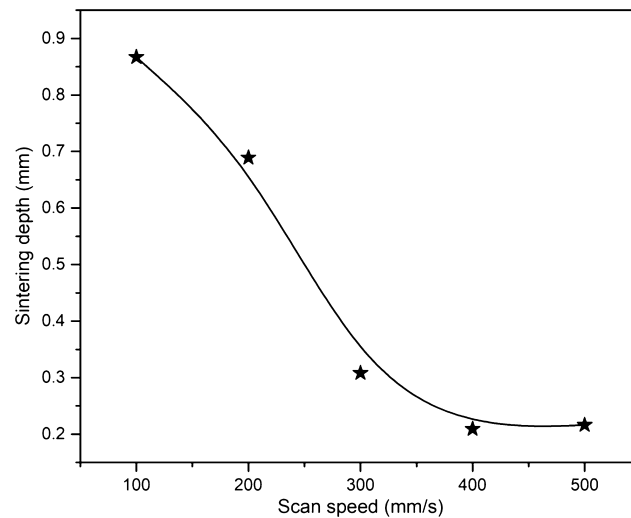
Fig. 12. Variation of the sintering depth with the scan speed.

4. Conclusion

A comprehensive three-dimensional transient thermal model for direct metal laser sintering of AlSi10Mg alloy was developed on an ANSYS platform. The model investigated the temperature distribution and sintering behavior of a AlSi10Mg built part with different laser power and scan speed values. Considering multiple modes of heat transfer and temperature-dependent thermo-physical properties, the following conclusions can be inferred:

(i) from the simulation results, it is quite evident that the process parameters and material properties have a great influence on the quality and property of the sintered part. With increasing the laser power, the temperature in the molten pool increases from 731 °C to 2672 °C, and the length and width of the molten pool also increases significantly;

(ii) with an increase in scan speed (100 mm/s to 500 mm/s), the temperature of the molten pool decreases from 1721 °C to 1162 °C due to the short interaction time of the laser beam with the powder bed;

(iii) the sintering depth of the powder bed increases from 0.061 mm to 0.872 mm with increasing laser power; a reverse phenomenon is observed with increasing scan speed. This will help to optimize the thickness of the powder layer for specific processing parameters and minimize the wastage of the excess powders;

(iv) from the current research, it can be concluded that optimization of the process parameters is necessary for obtaining a good-quality product having smooth surface finish, stability, and greater dimensional accuracy.

References

[1] W.E. Frazier, Metal additive manufacturing: a review, J. Mater. Eng. Perform. 23 (2014) 1917–1928.
[2] S. Sahoo, K. Chou, Phase-field simulation of microstructure evolution of Ti–6Al–4V in electron beam additive manufacturing process, Addit. Manuf. 9 (2016) 14–24.
[3] M.W. Khaing, J.Y.H. Fuh, L. Lu, Direct metal laser sintering for rapid tooling: processing and characterization of EOS parts, J. Mater. Process. Technol. 113 (2001) 269–272.
[4] J. Nandy, H. Sarangi, S. Sahoo, Microstructure evolution of Al–Si–10Mg in direct metal laser sintering using phase field modeling, Adv. Manuf. 6 (2018) 107–117.
[5] J. Romano, L. Ladani, M. Sadowski, Thermal modeling of laser based additive manufacturing processes within common materials, Proc. Manuf. 1 (2015) 238–250.
[6] Y. Tang, H.T. Loh, Y.S. Wong, J.Y.H. Fuh, L. Lu, X. Wang, Direct laser sintering of a copper-based alloy for creating three-dimensional metal parts, J. Mater. Process. Technol. 140 (2003) 368–372.
[7] A. Simchi, Direct laser sintering of metal powders: mechanism, kinetics and microstructural features, Mater. Sci. Eng. 428 (2006) 148–155.
[8] L. Dong, A. Makradi, S. Ahzi, Y. Remond, Three-dimensional transient finite element analysis of the selective laser sintering process, J. Mater. Process. Technol. 209 (2009) 700–706.
[9] K. Zeng, D. Pal, B. Stucker, A review of thermal analysis methods in laser sintering and selective laser melting, in: Proceedings of Solid Freeform Fabrication Symposium, Austin, TX, USA, vol. 60, 2012, pp. 796–814.
[10] X. Jian, S. Weimin, S.R. Rana, 3D modeling and testing of transient temperature in selective laser sintering (SLS) process, Optik 124 (2013) 301–304.
[11] Y. Li, D. Gu, Parametric analysis of thermal behavior during selective laser melting additive manufacturing of aluminum alloy powder, Mater. Des. 63 (2014) 856–867.
[12] P. Yuan, D. Gu, Molten pool behaviour and its physical mechanism during selective laser melting of TiC/AlSi10Mg nanocomposites: simulation and experiments, J. Phys. D, Appl. Phys. 48 (2015) 1–16.
[13] Q. Shi, D. Gu, M. Xia, S. Cao, T. Rong, Effects of laser processing parameters on thermal behavior and melting/solidification mechanism during selective laser melting of TiC/Inconel 718 composites, Opt. Laser Technol. 84 (2016) 9–22.
[14] H. Hu, X. Ding, L. Wang, Numerical analysis of heat transfer during multi-layer selective laser melting of AlSi10Mg, Optik 127 (2016) 8883–8891.

[15] E. Kundakcioglu, I. Lazoglu, S. Rawal, Transient thermal modeling of laser-based additive manufacturing for 3D freeform structures, Int. J. Adv. Manuf. Technol. 85 (2016) 493–501.

[16] W.-H. Lee, Y. Zhang, J. Zhang, Discrete element modeling of powder flow and laser heating in direct metal laser sintering process, Powder Technol. 315 (2017) 300–308.

[17] X. Zhao, A. Iyer, P. Promoppatum, S.-C. Yao, Numerical modeling of the thermal behavior and residual stress in the direct metal laser sintering process of titanium alloy products, Addit. Manuf. 14 (2017) 126–136.

[18] L. Dong, J.P.M. Correia, N. Barth, S. Ahzi, Finite element simulations of temperature distribution and of densification of a titanium powder during metal laser sintering, Addit. Manuf. 13 (2017) 37–48.

[19] A. Ojha, M. Samantaray, D.N. Thatoi, S. Sahoo, Continuum simulation of heat transfer and solidification behavior of AlSi10Mg in direct metal laser sintering process, IOP Conf. Ser., Mater. Sci. Eng. 338 (2018) 1–6.

[20] I.A. Roberts, C.J. Wang, A three-dimensional finite element analysis of the temperature field during laser melting of metal powders in additive layer manufacturing, Int. J. Mach. Tools Manuf. 49 (2009) 916–923.

[21] J. Nandy, H. Sarangi, S. Sahoo, Modeling of microstructure evolution in direct metal laser sintering: a phase field approach, IOP Conf. Ser., Mater. Sci. Eng. 178 (2017) 1–8.

[22] R.H. Bogaard, P.D. Desai, H.H. Li, C.Y. Ho, Thermophysical properties of stainless steels, Thermochim. Acta 218 (1993) 373–393.